Journal of Applied Polymer Science

Crystallization Behavior of Spray-Dried and Freeze-Dried Graphene Oxide/Poly(trimethylene terephthalate) Composites

Chengxin Guo, Liangliang Ji, Yaowen Li, Xiaoming Yang, Yingfeng Tu
Jiangsu Key Laboratory of Advanced Functional Polymer Design and Application, College of Chemistry, Chemical Engineering and Materials Science, Soochow University, Suzhou 215123, People's Republic of China
Correspondence to: Y. Tu (E-mail: tuyingfeng@suda.edu.cn) or X. Yang (E-mail: yangxiaoming@suda.edu.cn)

ABSTRACT: Two types of graphene oxide (GO) powders were prepared by freeze-drying or spray-drying method, and their composites with poly(trimethylene terephthalate) (PTT) were prepared by melt blending. The influence of GO powders' type and content on crystallization behavior of PTT was investigated by differential scanning calorimeter (DSC) and polarized optical microscopy (POM). DSC results indicated that the overall crystallization rate of PTT was accelerated by well-dispersed GO material which acts as a heterogeneous nucleation agent, since the Avrami parameter obtained is near 3. On the contrary, large GO aggregates which is in the minority will hinder the nucleation. Interestingly, large and well-defined PTT spherulites instead of tremendous stunted spherulites were observed from POM, which means only a small portion of GO powders was acted as nucleation agent. Meanwhile, GO powders had no effect on PTT spherulites growth rate. In addition, the band spacing of PTT spherulites became weaker and wider with increasing GO content. © 2014 Wiley Periodicals, Inc. J. Appl. Polym. Sci. **2014**, *131*, 40332.

KEYWORDS: blends; crystallization; composites; polyesters; differential scanning calorimetry (DSC)

Received 9 December 2013; accepted 17 December 2013
DOI: 10.1002/app.40332

INTRODUCTION

Poly(trimethylene terephthalate) (PTT) is a semicrystalline aromatic polyester with three methylene units in its monomer units and is a promising material for engineering applications such as films and fibers. PTT has not been studied in detail compared with poly(ethylene terephthalate) (PET) or poly(butylene terephthalate) (PBT) because PTT was not readily available until 1990s.[1] Considering that PTT is a semicrystalline polymer, its mechanical and physical properties are governed by the supermolecular morphology, which is in turn controlled by the crystallization process. Therefore, a deep understanding of the crystallization behavior is necessary from both fundamental and applied points of view. A lot of study focusing on the cold crystallization[2,3] and the melt crystallization[4–10] of PTT have been published in recent decades. Specially, spherulite morphology and interference color of PTT could be easily studied because it can form large, well-defined, and high refringent spherulites unlike PET and PBT.

A well-known approach for improving physical and mechanical properties of polymers is to introduce fillers. For this purpose, carbon nanotubes (CNTs),[11–14] graphene,[11,15] and clay,[16–20] which exhibit excellent physical properties, appear as excellent candidates to make advanced functional composite materials. Investigation of the influence of fillers on the crystallization behavior of PTT is promising. The interaction force between fillers and the semicrystalline polymer host may potentially alter the crystallization kinetics and the crystalline morphology of the latter. For polymer/inorganic filler composite materials, the fillers play a very important role on the nucleation and spherulite growth. To date, it has been found that particles act differently on nucleation process and spherulite growth stage.[20] Some particles can be efficient nucleating agents and some can act as physical barriers to the diffusion of the chains. In terms of fillers, one-dimensional CNTs and two-dimensional (2D) clay have been widely accepted as effective nucleating agents that facilitate the crystallization of various polymers.[14,15] Recently, taking graphene as filler is receiving more and more attention.[21–23] As a kind of layered material produced by the oxidation of graphite, graphene oxide (GO) has drawn a great deal of interests in various applications since the discovery of graphene in 2004 by Novoselov et al.[24,25] for its chemical polarity, a lamellar structure material similar with clay, and excellent miscibility with polymer such as PTT. However, there is no study reporting the crystallization behavior of PTT/GO composites. Up to now, investigations on polyester/GO composites were mainly focused on the improvement of mechanical strength[26,27] instead of

Additional Supporting Information may be found in the online version of this article.

crystallization kinetics. Yano et al. found that the modulus of crystalline PLA is increased from 3.3 GPa to 4.0 GPa and the strength from 50.2 MPa to 60.9 MPa, while the strain at break is reduced from around 7 to 3% compared with the amorphous PLA.[28] In Gagnon's research, the crystallization temperature greatly affected the mechanical properties of a thermoplastic elastomer produced by *Pseudomonas oleovorans*.[29] In brief, further investigation focusing on the mechanical properties and gas barrier properties must be interesting and hopeful. In previous reports, exfoliated graphite,[30] GO,[31] and graphene[26] can be successfully applied in the improvement of mechanical properties or moisture permeability. The lamellar structure and excellent miscibility with polymer indicates the optimistic prospect of using GO as filler for reinforcement like traditional clay. However, investigations on PTT/GO composites were mainly focused on the crystallization kinetics in this article because a deep understanding of the crystallization behavior is necessary from both fundamental and applied points of view.

It is well known that PTT can only be dissolved into strong polar solvents such as hexafluoroisopropanol, trifluoroacetic acid or 1 : 1 mixture of trifluoroacetic acid, and dichloromethane. Solvent mixing, however, is not an appropriate method for large scale PTT/GO composites preparation. Melt blending, a kind of low-cost and environmentally friendly method, was used to prepare PTT/GO composite in this study. In addition, it is very important to prepare uniform GO powders which have large specific surface area. Two kinds of well-dispersed GO powders prepared by freeze-drying and spray-drying method were used to prepare PTT/GO composites. The crystallization behavior of PTT/GO was investigated using differential scanning calorimeter (DSC) and polarized optical microscopy (POM). The nonisothermal and isothermal crystallization kinetics of polymer blends and its spherulite growth mechanism were studied. The spherulitic morphology was clearly studied by POM, and the influences of GO content on the spherulitic band structure were investigated as well.

EXPERIMENTAL

Materials

PTT was kindly supplied by DuPont Company. The density and melting peak temperature were 1.3 g/cm^3 and 228°C, respectively. Graphite powder and all the other reagents were purchased from Sinopharm Chemical Reagents Co., China. All reagents were used as received without further purification.

Preparation of GO Powders

GO solids were synthesized from graphite powders using a modified Hummers method.[32] Spray-dried graphene oxide powders (SGO) were prepared using a spray-dried machine (SP-1500, Shanghai Sunyitech Co., China). The detailed experimental process was as follows: the solvent feeding rate was 400 mL/hr, the air inlet temperature was 180°C, and the draught fan frequency was 50 Hz. Freeze-dried graphene oxide powers (FGO) were prepared using a Labconco FreeZone Freeze Dry System.

Preparation of PTT/GO Composites

The PTT/GO composites were prepared by melt blending method. PTT were dried in a vacuum oven for 12 hr at 110°C to avoid moisture induced hydrolysis reactions. Two series of PTT-based composites containing various SGO or FGO contents of 0.1, 0.3, 0.5, 1.0, and 5.0 wt % were prepared. PTT/SGO-X and PTT/FGO-X represent the composites with different types of GO. X represents the weight percent of GO in the composites. The temperature of co-rotating twin screw extruder with screws of 42 mm diameter and L/D = 36 was 230°C–235°C. The screw speed was 140 rpm.

Characterization

X-ray diffraction (XRD) patterns were acquired to characterize composite structure at room temperature by an X'PertPro MPD with a Cu-$K\alpha$ radiation source ($\lambda = 0.154$ nm). Before analysis, composites were pressed into 2 mm sheets. A 2θ range 5°–80° was selected to cover all the intense crystalline and amorphous peaks of PTT.

Fourier-transform infrared spectra (FTIR) of the power samples were recorded with a 3600 FTIR spectrometer. FTIR spectra were recorded at a resolution of 2 cm^{-1} and 16 scans from 4000 to 400 cm^{-1}.

Thermogravimetric analysis (TGA) experiments were carried out under nitrogen atmosphere with a Perkin Elmer Thermal Analyzer at a heating rate of 10°C/min.

The morphology of nanocomposites was investigated by scanning electron microscopy (SEM) using an Hitachi S4800 apparatus. The micrographs were taken from the cross section of samples previously immersed into liquid nitrogen.

Transmission electron microscopy (TEM, TecnaiG^{2}20, FEI) was employed to investigate the dispersion of GO in PTT. The samples were microatomed to ultrathin sections using a Leica UC7-FC7 Ultratome and transferred onto copper grid for observation.

The nonisothermal and isothermal crystallization behavior was investigated on a DSC (TA-Q200) with nitrogen as purge gas. Aluminum sample pans were used for all samples. The sample was prepared by quenching from the melt into liquid nitrogen before the measurement. The sample weight was in the range of 5–10 mg. During the nonisothermal crystallization, the samples were directly cooled to −20°C and then heated to 280°C at a heating rate of 10°C/min, followed by cooling to −20°C at a rate of 10°C/min and reheated using the same rate. Isothermal crystallization was conducted by following steps: at first the samples were heated from 30°C to 280°C at 10°C/min, then maintained at 280°C for 5 min, at last quenched (100°C/min) from 280°C to a desired isothermal crystallization temperature, T_c (190°C, 195°C, 200°C, 205°C, and 210°C), and maintained at T_c until crystallization was completed.

POM observations were carried out on a polarizing microscope (Olympus Corporation, BX51-P) at a magnification (×200) which was coupled with a computer-controlled video camera. A dual hot stage (Linkam THMS600) was used for controlling the temperature. The heating and cooling procedures were the same as that used in the isothermal DSC analysis. Visual observations of crystallization behavior of spherulites under 200°C were carried out on the POM equipped with an Qimaging camera to measure the light intensity as well. The camera possesses 16-bit dynamic range charge-coupled detector (CCD) with a

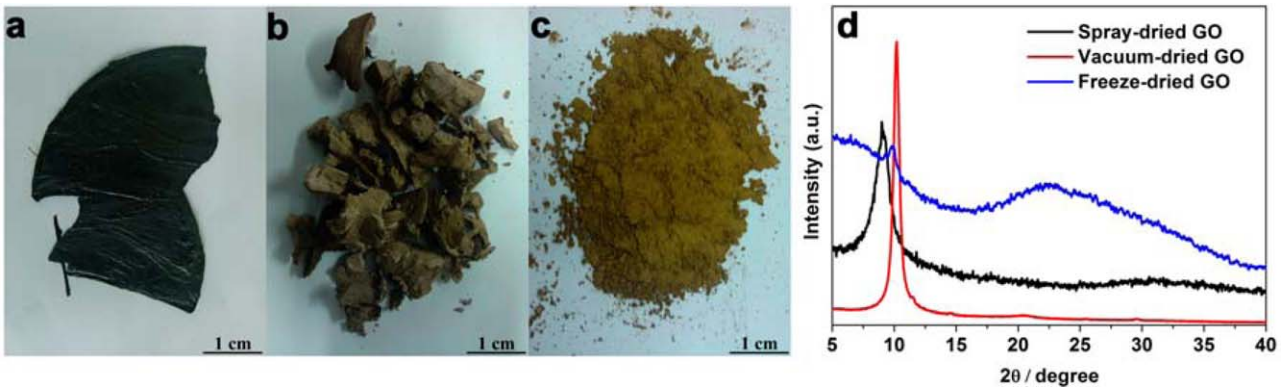

Figure 1. Photographs of (**a**) vacuum-dried GO; (**b**) freeze-dried GO; (**c**) spray-dried GO, and (**d**) WAXS patterns for various GO dried by different methods. [Color figure can be viewed in the online issue, which is available at wileyonlinelibrary.com.]

resolution of 2048 × 1536 pixels. Automatic storage of the images was conducted by a recording system at a time interval of 0.3 s. Under cross-polars, the high-performance CCD imaging system will give the intensity change of transmitted light of selected regions enclosing the desired spherulite separately. The transmitted light intensity was thus monitored as a function of time. In addition, the maximum transmitted light intensity is normalized together.

RESULTS AND DISCUSSION

Figure 1 shows the photographs and XRD patterns of GO dried by different method. GO dried by vacuum were too hard to be grounded [Figure 1(a)]. Thus, homogeneous PTT/GO composite could not be obtained by melt blending method. To exploit more availability of the GO materials, we prepared the GO powders from their colloidal suspensions by two other methods. By a freeze-drying method, the suspensions were converted to solid foams, as shown in Figure 1(b). By a spray-drying method, the suspensions were converted to powders, as shown in Figure 1(c). Homogeneous PTT/GO composite was successfully prepared using these two kinds of GO.

The structures of three kinds of GO materials were investigated using XRD [Figure 1(d)]. In case of vacuum-dried GO, a diffraction peak at 10.2° was observed, corresponding to a distance of 8.7 Å, which means the interlayer distance between GO sheets. For the SGO, a peak at 2θ of 9.0° was observed, which corresponds to an interlayer distance of 9.8 Å. The increase of the layer distance indicates a weak interaction between SGO layers, which was supported by the appearance of SGO powders, where SGO appeared dark brown while vacuum died GO appeared black. A weak interaction between the GO layers will be more useful in industrial application since the GO sheets are easier to be exfoliated. The FGO processed with freeze-drying technique shows a relative flat diffraction pattern and a weak peak around 9.9°, which indicated that the ordered structures is low.[33–35]

Fine and uniform dispersion of GO sheets and strong interfacial interaction are two major criteria governing the good mechanical properties and crystallization behavior of composites. From Supporting Information Figure S1(a) and Table SI, we can see that SGO still possess a large number of oxygenated functional groups even after thermal treatment (240°C). In our opinion, a strong interaction between PTT and GO is expected owing to the presence of hydrogen bonds between the PTT and the remaining oxygenated groups of GO [Supporting Information Figure S1(b)].[31] In addition, interaction could be strengthened via esterification reaction[36,37] between hydroxyl groups and carboxyl groups of PTT and GO.

According to Supporting Information Figure S2, the PTT/FGO-0.1 and PTT/SGO-0.1 illustrate a very smooth surface[31] with some stripes in the fracture direction whereas the incorporation of larger GO sheets into the polymer resulted in the formation of many irregular protuberances evenly distributed on the fracture surface. Judging from the fact that some sheets are directly exposed on the fracture surface, we can assume that PTT/SGO are better dispersed and oriented with less aggregation compared with that of PTT/FGO. More importantly, the composite made from high FGO content over 5 wt % [Supporting Information Figure S2(c)] revealed much more significant reaggregation than that of 5 wt % SGO [Supporting Information Figure S2(c′)]. Meanwhile, the TEM images (Supporting Information Figure S3) and light microscopy images (Supporting Information Figure S4) of PTT/SGO composites also show less aggregates and better dispersion than that of PTT/FGO composites.[14,38] These reaggregations was also confirmed by the results from WAXS (Supporting Information Figure S5) that PTT/FGO-5 and PTT/SGO-5 shows weaker crystalline intensity. In conclusion, the dispersion state of SGO is much better than that of FGO which also has been confirmed by the following isothermal DSC tests.

To investigate the crystallization behavior of PTT/GO composites, we performed nonisothermal and isothermal DSC tests in detail. Figure 2 shows nonisothermal crystallization results for PTT and the composites. The results for the crystallization and thermal parameters are reported in Table I. Glass transition temperature values (T_g), measured prior to crystallization, are also shown in Table I. A very small difference only appears in the T_g of PTT and composites. The values are close to 46°C. The addition of GO induces no measurable change in the glass transition temperature. Because of the melt quenching in liquid nitrogen, all the samples show obvious T_{cc}, the temperature of which slightly decreased with the addition of GO.

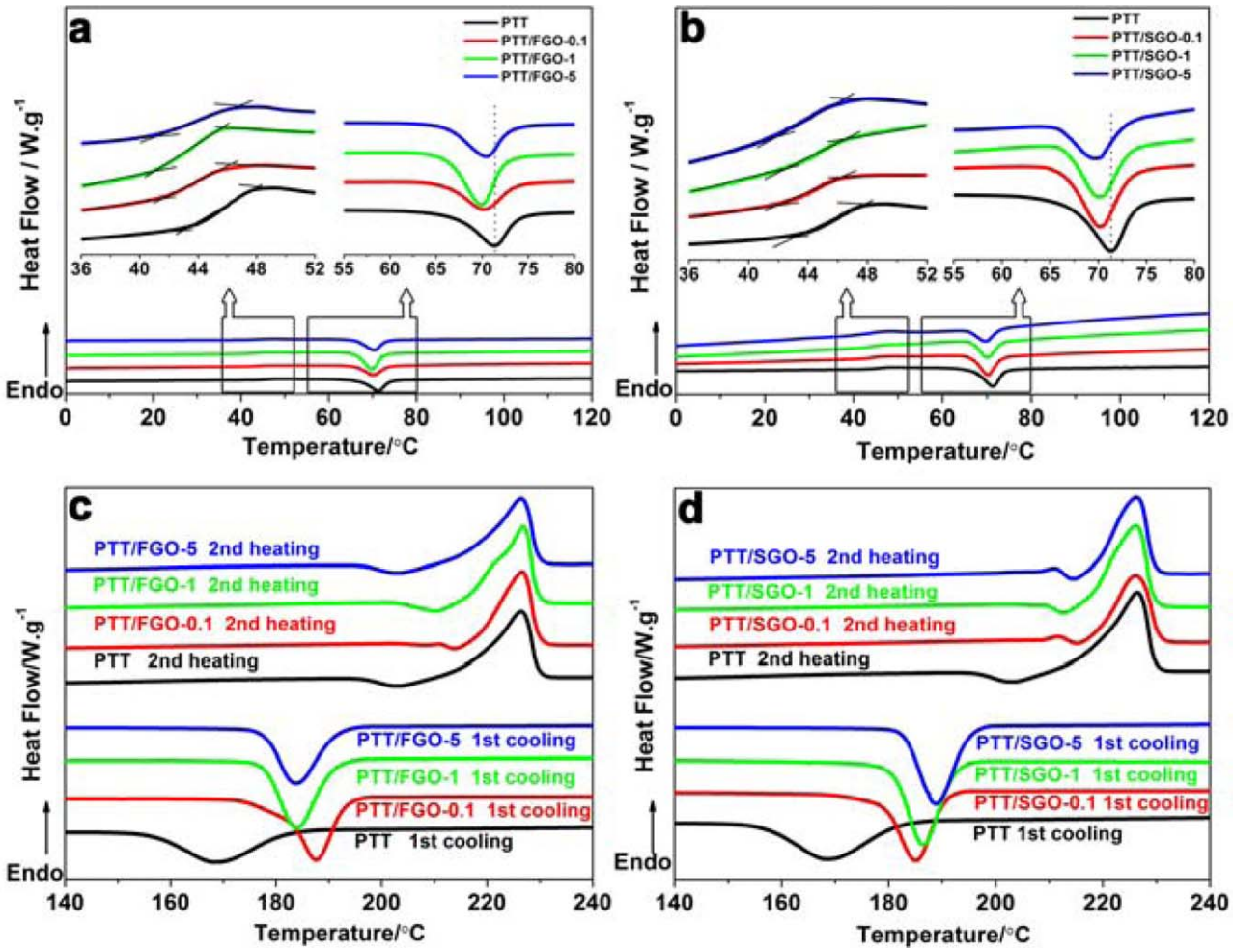

Figure 2. DSC thermograms for (**a**) PTT/FGO (0°C–120°C), (**b**) PTT/SGO (0°C–120°C) (**c**) PTT/FGO (140°C–240°C), and (**d**) PTT/SGO (140°C–240°C). [Color figure can be viewed in the online issue, which is available at wileyonlinelibrary.com.]

As for melt crystallization, it is evident that there is a distinct exothermic crystallization peak in all of the cooling scans. The T_{mc}'s for composites are higher than that of neat PTT. The increase of T_{mc} and ΔH_{mc} confirmed that the overall crystallization is accelerated for the presence of GO [Figure 2(c,d); Table I]. Interestingly, crystallization cannot be accelerated illimitably because the excessive increase of filler causes large aggregation. For PTT/FGO composites, despite their higher T_{mc} than that of pure PTT, the peaks of PTT/FGO-5 significantly shifted to the lower temperature compared with that of PTT/FGO-0.1 as is shown in Figure 2(c). This means the melt crystallization was slightly impacted with the introduction of 5 wt % FGO, which could be attributed to that FGO aggregations limited the nucleation and segment mobility of polymer matrix. The inhibition effect was also supported by the melting curve of PTT/FGO-5 [Figure 2(c)] that the endothermic peak, similar to that of neat PTT, is a little broader. The decrease of ΔH_m and ΔH_{mc} at high filler content (5 wt %), suggests a lower crystallinity with imperfect spherulites which originated from the destructive effect of FGO aggregation, and this phenomenon happens to coincide with the PTT/exfoliated graphite system.[30]

On the contrary to FGO fillers, T_{mc} increases gradually with the increase of SGO content, as indicated in Figure 2(d). A regular T_{mc} increased with SGO content shows that the better dispersed SGO powders acted as an excellent nucleating agent in a heterogeneous nucleation process. Such effects have also been reported

Table I. Values of T_g, T_{cc}, T_m, ΔH_m, T_{mc}, and ΔH_{mc} for PTT, PTT/FGO, and PTT/SGO Composites

Samples	T_g (°C)	T_{cc} (°C)	T_m (°C)	ΔH_m (J/g)	T_{mc} (°C)	ΔH_{mc} (J/g)
PTT	46.0	71.4	226.5	59.9	168.7	46.2
PTT/FGO-0.1	46.0	70.2	226.6	51.6	187.6	50.6
PTT/FGO-1	45.8	68.9	226.9	53.8	184.0	53.3
PTT/FGO-5	45.7	70.4	226.8	50.4	183.8	47.7
PTT/SGO-0.1	45.7	70.0	226.1	51.0	185.1	48.1
PTT/SGO-1	45.7	70.8	226.2	51.9	186.5	48.4
PTT/SGO-5	45.5	70.2	226.2	47.3	188.9	46.3

ΔH_m and ΔH_{mc} values in Table I are for the unit weight of PTT part in the composite.
T_g, glass transition temperature; T_{cc}, cold crystallization temperature; T_m, melting temperature; ΔH_m, melting enthalpy; T_{mc}, melt crystallization temperature; ΔH_{mc}, melt crystallization enthalpy.

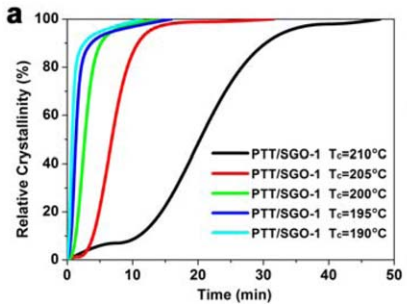

b

$t_{1/2}$ (min)	T_c				
	190 °C	195 °C	200 °C	205 °C	210 °C
PTT	9.0	11.2	18.5	36.0	50.9
PTT/SGO-0.1	1.2	1.6	2.3	4.7	12.2
PTT/SGO-1	1.2	1.6	2.7	5.6	12.3
PTT/SGO-5	1.5	1.8	3.1	6.2	15.2

Figure 3. (**a**) Relative crystallinity as a function of time for PTT/SGO-1 at various temperatures. (**b**) The half-crystallization time $t_{1/2}$ of PTT and PTT/SGO composites. [Color figure can be viewed in the online issue, which is available at wileyonlinelibrary.com.]

in previous literatures.[18,39] Thus, it can be concluded that the dispersion state of the filler is very important for the crystallization behavior of polymer matrix, since well-dispersed fillers will promote heterogeneous nucleating, while large filler aggregation will hinder the crystallization.

Figure 3(a) shows the relative crystallinity versus time curves of PTT/SGO-1 at 190°C, 195°C, 200°C, 205°C, 210°C, respectively. Figure 3(b) lists the half-time of crystallization, $t_{1/2}$, with different SGO content. The crystallization rates of PTT and composites become slower as the isothermal crystallization temperature (T_c) increases. As shown in Figure 3(b), the $t_{1/2}$ decreases (i.e., crystallization rate increases) with SGO in the composites. These results imply that the crystallization rate of PTT was accelerated by SGO. It is worthy to note that when T_c is higher than 200°C, PTT/SGO-5 exhibits significant slower crystallization rate (higher $t_{1/2}$ value) than the other samples, which is due to the barrier effect of SGO aggregates. Similar trend was observed from the PTT/FGO composite but the data was not shown here. In addition, the intensity transmitted versus time through the sample between crossed polarizers was recorded during the experiments (Supporting Information Figure S7).

The Avrami equation was employed to analyze the isothermal crystallization in order to understand the role of GO on the nucleation or the growth of the PTT crystallites. The Avrami equation is given by[40,41]: $1-X(t)=\exp(-Kt^n)$. The crystallization kinetics was investigated at 200°C. This temperature was selected as a compromise between nucleation and growth of crystals because crystal nucleation is favored at low temperature when molecular mobility is low, whereas crystal growth is favored at high temperature when viscosity is low. Table II shows the Avrami parameters of PTT and PTT/SGO composites at crystallization temperature of 200°C. At this temperature, the Avrami exponent is 2.81 and around 2.9 for neat PTT and PTT/SGO composites, respectively. This temperature corresponds to an optimum for which the growth between 2D and three-dimensional (3D) is induced from instaneous nuclei ($n=2$–3) and/or sporadic nuclei ($n=3$). Huang and Chang found that the average Avrami value of PTT in the studied crystallization temperature is about 2.8.[42] The same results indicate that both the nucleation and growth mechanism of PTT and PTT/GO composites are the same in the crystallization temperature range investigated. Considering the Avrami equation, in the ideal state of nucleated crystallization for 3D crystallization growth, the n value should be exactly 3.[40] Thus, the obtained n values near 3 suggest 3D crystallization growth in our studied system, which will produce spherulitic morphology, as is consistent with the POM images shown as Figure 4.

The spherulite growth morphologies of PTT and PTT/GO composite were observed using POM in order to understand the effect of filler. Figure 4 shows a series of POM observations of the samples crystallized at various isothermal crystallization temperatures. All the samples show a relatively well-defined spherulitic texture with clear Maltese crosses. For pure PTT and its blends, fairly large and perfect spheroids are grown with a clear Maltese cross. The positive Maltese cross pattern indicates along or perpendicular to orientation of the crystalline molecular axis with respect to spherulitic radius.[43] According to the other polymer modified by clay, CNT, or GO[12,19,21] their spherulites are smaller in size and larger in number than those of the neat polymer. Herein, as shown in Figure 4 the number of spherulites is increased in the order of PTT < PTT/SGO-0.1 < PTT/SGO-1 except PTT/SGO-5. The reason is that well-dispersed fillers could act effectively as nucleation agent but large aggregates could not. Simultaneously, GO content and dispersion state in polymer matrix have no effect on the spherulite growth of PTT. As shown in Figure 4, the poorly-dispersed PTT/FGO-5 aggregation composite also show well-defined spherulites.

Although the overall crystallization rate of PTT increases in the presence of GO according to the nonisothermal and isothermal DSC tests, the growth rate of spherulites exhibits a quite different tendency through the POM observation. By following the variation of radius of PTT spherulites with crystallization time, the spherulitic growth rates were estimated for both neat PTT and the composites with a same GO loading at different temperature. Figure 5(a) shows the various spherulitic size of PTT/SGO-0.1 sample at different crystallization temperature corresponding to the plots of spherulite radius versus crystallization

Table II. Avrami Parameters of PTT and PTT/SGO Composites at 200°C

	PTT	PTT/SGO-0.1	PTT/SGO-0.3	PTT/SGO-0.5	PTT/SGO-1	PTT/SGO-5
n	2.81	2.85	2.84	2.87	2.88	2.92

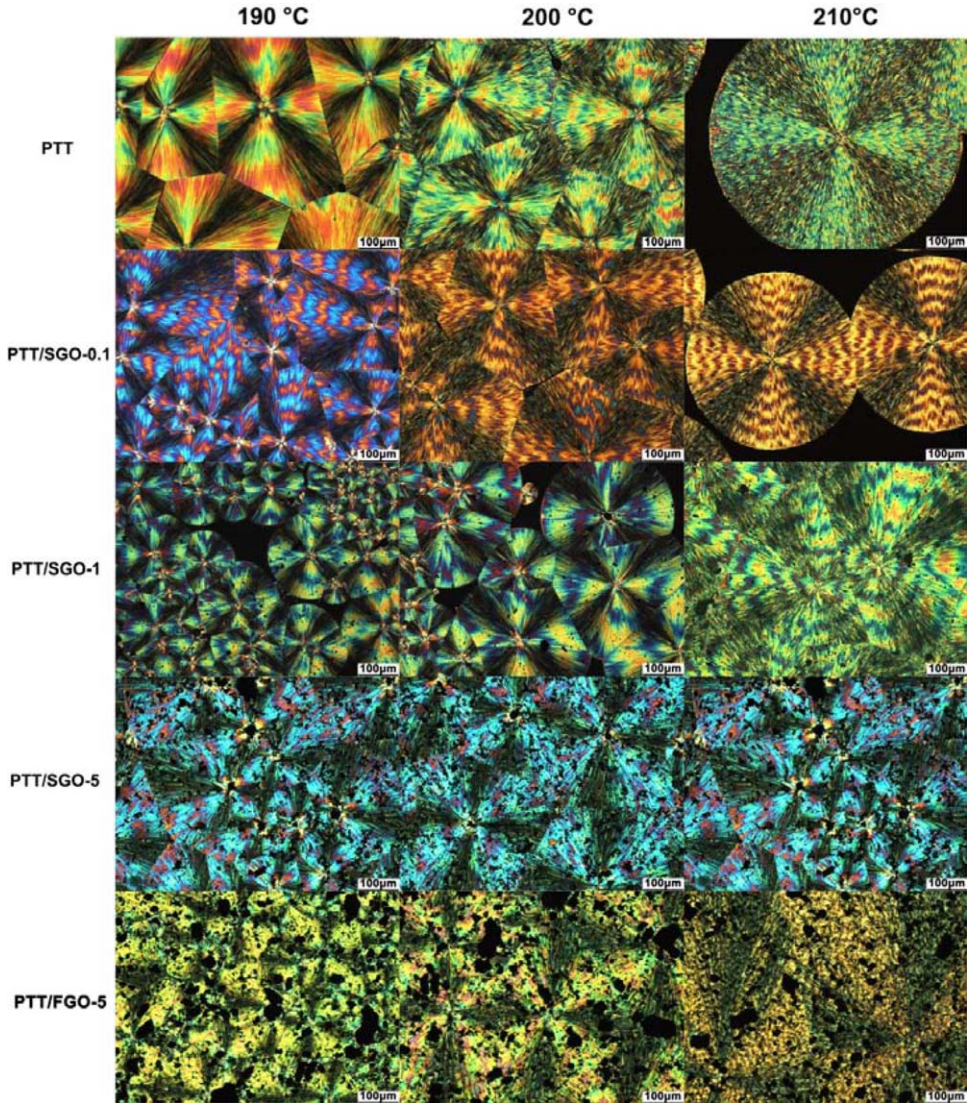

Figure 4. POM images of PTT, PTT/SGO-0.1, PTT/SGO-1, PTT/SGO-5, and PTT/FGO-5 samples crystallized at different crystallization temperatures from the melt. [Color figure can be viewed in the online issue, which is available at wileyonlinelibrary.com.]

time. The solid lines represent the best linear fits of least-squares method to the data. Apparently, there is a linear increase in the radius with time until the spherulites impinge on adjacent single crystals and suppress the crystal growth. It can also be observed that the induction time for nucleation became larger at higher crystallization temperature. Actually in

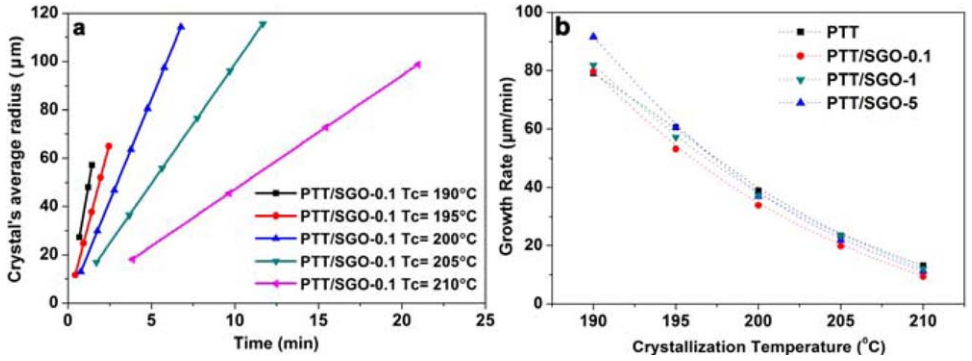

Figure 5. (**a**) Average radius of PTT/SGO-0.1 spherulites as a function of time. (**b**) Spherulite growth rate of pure PTT and PTT/SGO samples as a function of crystallization temperature. [Color figure can be viewed in the online issue, which is available at wileyonlinelibrary.com.]

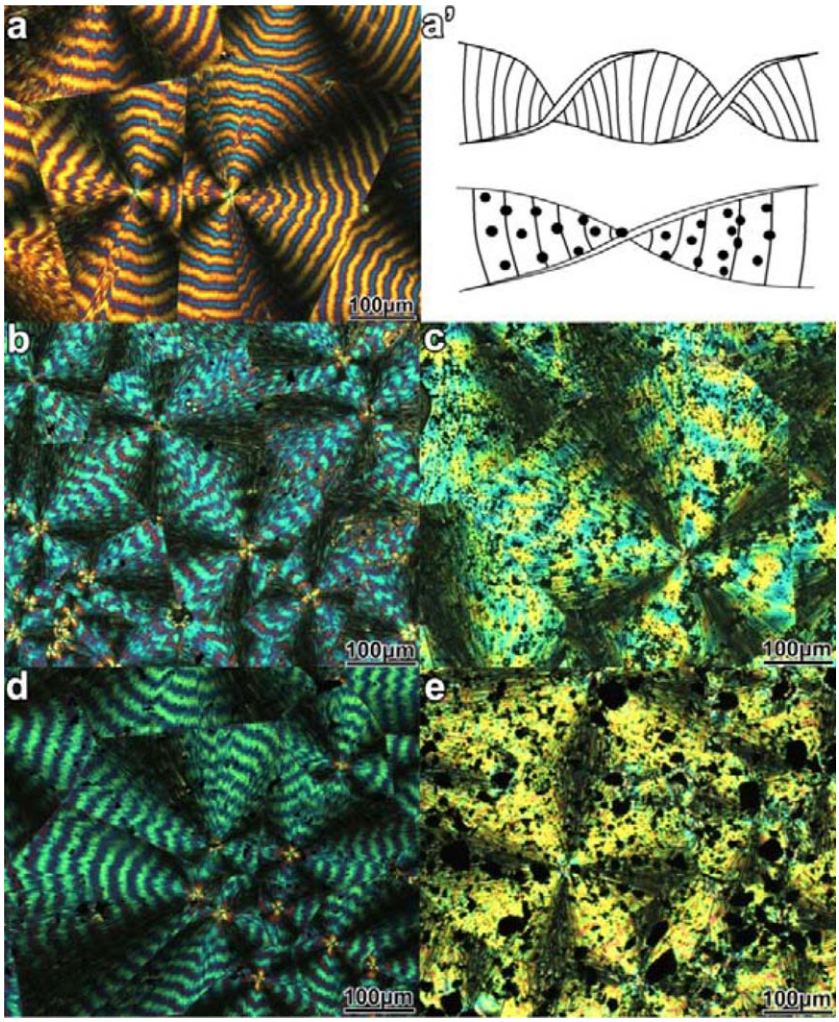

Figure 6. POM images of (**a**) pure PTT, (**a′**) the twining mechanism of the intralamellar model in PTT and its blends, (**b**) PTT/SGO-0.5, (**c**) PTT/SGO-5, (**d**) PTT/FGO-0.5, and (**e**) PTT/FGO-5 after isothermal crystallization at $T_c = 175°C$. [Color figure can be viewed in the online issue, which is available at wileyonlinelibrary.com.]

previous report about CNT fillers,[11] the induction time was also shortened with the addition of CNTs. The spherulitic growth rates were measured from neat PTT and its composites. Figure 5(b) shows spherulite growth rate seems to be about the same at an equal temperature, which has been calculated ranging from 0.15 to 1.56 μm/s. The presence of GO influence the spherulitic morphology by acting as nucleating agent but little effect on the spherulitic growth rates of PTT in the PTT/GO composites. In conclusion, the addition of SGO or FGO (data not shown) induces no measurable change in the spherulite growth rate under the same T_c. So we can make sure that the accelerated crystallization behavior is due to the heterogeneous nucleation of GO.

The banded structures are observed clearly in the spherulites of pure PTT and the composites. Given the chosen crystallization temperatures, morphological changes of all the samples show the same trend, spherulite without band is formed at low and extremely high temperature, and band structure is formed at the middle temperature. During observation, PTT spherulites crystallized at range from 160°C to 180°C show obvious banded structures. Figure 6 shows the POM images of banded spherulites of PTT and PTT/GO composites at 175°C.

It was found that banded structure of the PTT spherulite was caused by lamellar twisting which generates alternating flat-to-edge-on morphology.[44] The driving force of lamellar twisting probably originates from the unbalanced stress at lamellar surface. Moreover, until now there are few reports about the influence of fillers on the banded structure of PTT. It has been reported that the band spacing decreased in the presence of fillers.[45,46]

The influence of GO on the banded structure of PTT was investigated in this study. Figure 6(a–e) shows the spherulitic textures formed at 175°C. The Maltese cross and banding can be clearly seen in these images. These lamellar fibrils spirally protrude from the center of spherulites. The interference color of the spherulites is related to the film thickness.[5] It was found that the width of band spacing changes with the thickness of sample,[8] so the thickness was kept as same as possible in this study. Both the PTT/SGO and PTT/FGO systems have a similar trend: the band spacing became weaker and wider in the

presence of GO. In conclusion, the GO aggregation exhibits a synergistic effect on destroying the formation of banded structure. The reason is that larger GO aggregation can destroy the chain folding and lamellae twisting [Figure 6(a′)].

CONCLUSIONS

In this study, PTT/GO composites with different contents of GO show different crystalline behavior from those of PTT. Two kinds of GO (FGO and SGO) were used and investigated. FGO and SGO have the same effect on the crystallization behavior of PTT except that sometimes there is variation in the system of high GO content due to the poorly-dispersed state in polymer matrix. The presence of GO has little effect on the crystalline structure of the PTT. DSC measurements reveal that there is no significant variation of T_g, T_{cc}, and T_m for different samples. The increase of T_{mc} with the increase of SGO content shows that the dispersed SGO powders act as an excellent nucleating agent in a heterogeneous nucleation process. Although the overall crystallization rate of PTT increases in the presence of GO, the growth rate of spherulites exhibits the same. GO as a mild nucleation agent could be used to adjust the crystallization behavior of PTT, which offers helpful guidance to control the crystallization of polymer/inorganic filler composites.

ACKNOWLEDGMENTS

The financial support from the National Nature Science Foundation of China (No. 21104050), a Project Funded by the Priority Academic Program Development of Jiangsu Higher Education Institutions, the Educational Bureau of Jiangsu Province (No: 10KJB430013), China Postdoctoral Science Foundation (2013M541715) and Natural Science Foundation of Jiangsu Province of China (General Program BK2011356) are gratefully acknowledged.

REFERENCES AND NOTES

1. Traub, H. L.; Hirt, P.; Herlinger, H.; Oppermann, W. *Angew. Makromol. Chem.* **1995**, *4055*, 179.
2. Sanz, A.; Nogales, A.; Ezquerra, T. A.; Soccio, M.; Munari, A.; Lotti, N. *Macromolecules* **2010**, *43*, 671.
3. Chuang, W. T.; Su, W. B.; Jeng, U. S.; Hong, P. D.; Su, C. J.; Su, C. J.; Su, C. H.; Huang, Y. C.; Laio, K. F.; Su, A. C. *Macromolecules* **2011**, *44*, 1140.
4. Chuah, H. H. *Polym. Eng. Sci.* **2001**, *41*, 308.
5. Chen, H. B.; Chen, L.; Zhang, Y.; Zhang, J. J.; Wang, Y. Z. *Phys. Chem. Chem. Phys.* **2011**, *13*, 11067.
6. Hong, P. D.; Chung, W. T.; Hsu, C. F. *Polymer* **2002**, *43*, 3335.
7. Chuang, W. T.; Hong, P. D.; Chuah, H. H. *Polymer* **2004**, *45*, 2413.
8. Wang, B. J.; Li, C. Y.; Hanzlicek, J.; Cheng, S. Z. D.; Geil, P. H.; Grebowicz, J.; Ho, R. M. *Polymer* **2001**, *42*, 7171.
9. Patel, D.; Bassett, D. C. *Polymer* **2002**, *43*, 3795.
10. Sasaki, S.; Sakaki, Y.; Takahara, A.; Kajiyama, T. *Polymer* **2002**, *43*, 3441.
11. Xu, J. Z.; Chen, T.; Yang, C. L.; Li, Z. M.; Mao, Y. M.; Zeng, B. Q.; Hsiao, B. S. *Macromolecules* **2010**, *43*, 5000.
12. Barrau, S.; Vanmansart, C.; Moreau, M.; Addad, A.; Stoclet, G.; Lefebvre, J. M.; Seguela, R. *Macromolecules* **2011**, *44*, 6496.
13. Miltner, H. E.; Grossiord, N.; Lu, K.; Loos, J.; Koning, C. E.; Mele, B. R. *Macromolecules* **2008**, *41*, 5753.
14. Leelapornpisit, W.; Ton-That, M. T.; Perrin-Sarazin, F.; Cole, K. C.; Denault, J.; Simard, B. *J. Polym. Sci. Part: B. Polym. Phys.* **2005**, *43*, 2445.
15. Xu, J. Z.; Chen, C.; Wang, Y.; Tang, H.; Li, Z. M.; Hsiao, B. S. *Macromolecules* **2011**, *44*, 2808.
16. Kim, B.; Lee, S. H.; Lee, D.; Ha, B.; Park, J.; Char, K. *Ind. Eng. Chem. Res.* **2004**, *43*, 6082.
17. Davis, C. H.; Mathias, L. J.; Gilman, J. W.; Schiraid, D. A.; Shields, J. R.; Trulove, P.; Sutto, T. E.; Delong, H. C. *J. Polym. Sci. Part: B. Polym. Phys.* **2002**, *40*, 2661.
18. Ou, C. F. *J. Polym. Sci. Part: B. Polym. Phys.* **2003**, *41*, 2902.
19. Maiti, P.; Nam, P. H.; Okamoto, M. *Macromolecules* **2002**, *35*, 2042.
20. Favaro, M. M.; Rego, B. T.; Branciforti, M. C.; Bretas, R. E. S. *J. Polym. Sci. Part: B. Polym. Phys.* **2010**, *48*, 113.
21. Hua, L.; Kai, W. H.; Inoue, Y. *J. Appl. Polym. Sci.* **2007**, *106*, 4225.
22. Liang, J. J.; Huang, Y.; Zhang, L.; Wang, Y.; Ma, Y. F.; Guo, T. Y.; Chen, Y. S. *Adv. Funct. Mater.* **2009**, *19*, 2297.
23. Kuilla, T.; Bhadra, S.; Yao, D. H.; Kim, N. H.; Bose, S.; Lee, J. H. *Prog. Polym. Sci.* **2010**, *35*, 1350.
24. Novoselov, K. S.; Geim, A. K.; Morozov, S. V.; Jiang, D.; Zhang, Y.; Dubonos, S. V.; Grigorieva, I. V.; Firsov, A. A. *Science* **2004**, *306*, 666.
25. Stankovich, S.; Dikin, D. A.; Dommentt, G. H. B.; Kohlhaas, K. M.; Zimmney, E. J.; Stach, E. A.; Piner, R. D.; Nguyen, S. T.; Ruoff, R. S. *Nature* **2006**, *442*, 282.
26. Bandla, S.; Hanan, J. C. *J. Mater. Sci.* **2012**, *47*, 876.
27. Bora, C.; Gogoi, P.; Baglari, S.; Dolui, S. K. *J. Appl. Polym. Sci.* **2013**, *129*, 3432.
28. Suryanegara, L.; Nakagaito, A. N.; Yano, H. *Compos. Sci. Technol.* **2009**, *69*, 1187.
29. Gagnon, K. D.; Lenz, R. W.; Farris, R. J.; Fuller, R. C. *Macromolecules* **1992**, *25*, 3723.
30. Li, M.; Jeong, Y. G. *Macromol. Mater. Eng.* **2011**, *296*, 159.
31. Yousefi, N.; Gudarzi, M. M.; Zheng, Q. B.; Lin, X. Y.; Shen, X.; Jia, J. J.; Sharif, F.; Kim, J. K. *Compos A* **2013**, *49*, 42.
32. Yang, X. M.; Tu, Y. F.; Li, L. A.; Shang, S. M.; Tao, X. M. *ACS Appl. Mater. Interf.* **2010**, *2*, 1707.
33. Cao, Y. W.; Feng, J. C.; Wu, P. Y. *Carbon* **2010**, *48*, 3834.
34. Huang, H.; Chen, P. W.; Zhang, X. T.; Lu, Y.; Zhan, W. C. *Small* **2013**, *9*, 1397.
35. Yang, X. W.; Zhu, J. W.; Qiu, L.; Li, D. *Adv. Mater.* **2011**, *23*, 2833.
36. Yang, J. H.; Lin, S. H.; Lee, Y. D. *J. Mater. Chem.* **2012**, *22*, 10805.
37. Badri, A.; Whittaker, M. R.; Zetterlund, P. B. *J. Polym. Sci. Part: A. Polym. Chem.* **2012**, *50*, 2981.

38. Ma, H. L.; Zhang, H. B.; Hu, Q. H.; Li, W. J.; Jiang, Z. G.; Yu, Z. Z.; Dasari, A. *ACS Appl. Mater. Interf.* **2012**, *4*, 1948.
39. Xing, C. Y.; Zhao, L. P.; You, J. C.; Dong, W. Y.; Cao, X. J.; Li, Y. J. *J. Polym. Sci. Part: B. Polym. Phys.* **2012**, *116*, 8312.
40. Avrami, M. *J. Chem. Phys.* **1940**, *8*, 212.
41. Binsbergen, F. L. *J. Macromol. Sci. Phys.* **1970**, *4*, 837.
42. Huang, J. M.; Chang, F. C. *J. Polym. Sci. Part: B. Polym. Phys.* **2000**, *38*, 934.
43. Samuels, R. J. *J. Polym. Sci. Part: B. Polym. Phys.* **1971**, *9*, 2165.
44. Ho, R. M.; Ke, K. Z.; Chen, M. *Macromolecules* **2000**, *33*, 7529.
45. Morra, B. S.; Stein, R. S. *J. Polym. Sci. Part: B. Polym. Phys.* **1982**, *20*, 2261.
46. Janimak, J. J.; Markey, L.; Stevens, G. C. *Polymer* **2001**, *42*, 4675.